

**Repeatability and Stiffness of Relocation Three V-grooves  
Kinematic Couplings for Precision Engineering**

**Mohammad S. Alsoufi**

Mechanical Engineering Department,  
College of Engineering and Islamic Architecture  
Umm Al-Qura University, Makkah, KSA  
E-mail: [mssoufi@uqu.edu.sa](mailto:mssoufi@uqu.edu.sa)



## Repeatability and Stiffness of Relocation Three V-grooves Kinematic Couplings for Precision Engineering

Mohammad S. Alsoufi

### ملخص البحث

تم استخدام أنظمة نقل الحركة (مثل كيلفن كلامب "Kelvin Clamp") والتي تستند إلى قيود حركة الأجسام الكروية على السطوح، بشكل واسع خلال العقود الماضية، بالإضافة إلى المراجع العلمية عن كيفية تصميمها واستخدامها. والمدهش عدم وجود بيانات أو معلومات كافية حول مثل هذه الأنظمة عن الأجسام متناهية الصغر (تقنية النانو) مثل الانتقال المتكرر للعينات المراد اختبارها وتحليلها والتي تتسم بمقاسات صغيرة جداً. من أجل ذلك، سوف نستعرض في هذا البحث نموذجاً تجريبياً وتحليلياً لأنظمة النقل الحركية في نطاق صغير جداً للوصول إلى نتائج تفيد في اختبار وتحليل عينات صغيرة عن علم الاحتكاك بين الأجسام متناهية الصغر.

وهذه الدراسة تبحث في دقة الانتقال والصلابة الساكنة لنظام كيلفن كلامب تحت مستويات مختلفة من القوى مثل قوة الإغلاق وقوة المحور المتصالب ويتم تقييم مدى صلابة نظام كيلفن كلامب مباشرة عن طريق التحرك الجزئي الناتج عن التحويلات الصغيرة في القوى الساكنة.

وسيتم تقديم نتائج لقضايا متعلقة بخصونة ونعومة السطوح المختلفة للمواد، وكذلك المواد اللازمة لهذه الأخاديد والتكلفة المادية واستخدام الأجهزة الصغيرة في الصناعة، بالإضافة إلى مناقشة الآثار المترتبة على هذه النتائج لنقوم بتصميم نموذج ذي تطبيق عملي على أنظمة كيلفن كلامب المتناهية الصغر.

## ABSTRACT

The basic mechanical behaviour of some low-cost miniature "Kelvin Clamp" devices has been investigated, addressing the lack of guidelines for such micro- and nano-systems. This study investigates the small-scale relocation precision and static stiffness of the T-geometry samples of steel and as-ground aluminium devices under various representative levels of closure force and cross-axis force. Clamp stiffness is evaluated directly in terms of micro-displacement induced by small modulations in the static forces. Typically the separation between ball contacts is around 5 mm. In all cases, the balls are standard commercial ones and usually smoother than the counterfaces that they contact. The test-rig is described. Low-cost small kinematic "Kelvin Clamps" are practical, with care. Polishing the grooves appears not to provide cost-effective improvements for the low-mass devices. In addition, the reader may find the kinematic coupling design presented in this paper useful for future applications of ultra-precision, wafer-to-wafer of micro-systems, particularly in MEMS/NEMS fields.

**Keywords:** miniature; Kelvin clamp; micro- and nano-systems; relocation; precision; kinematic, closure force, cross-axis force.

## 1. Introduction

Kinematic relocation devices (such as the "Kelvin clamp") based on ball-on-flat displacement constraints have been used for well over a century. The origin of the kinematic coupling dates back at least to 1,876 when James Clerk Maxwell described the three V-grooves coupling as a method to establish a definite position [1-3]. He also described the tetrahedron-Vee-flat coupling in use by William Thomson, now widely known as Lord Kelvin and hence the term 'Kelvin clamp'. Evans found evidence that both Maxwell and Thompson learned kinematics from Professor Robert Willis, but apparently Willis' own publications do not support him as the innovator [3]. In particular, Thompson mentions being taught the geometrical (or kinematic) method by Willis some thirty years earlier, approximately 1,849 [4]. Regardless of the origin, in the measurement and instrumentation fields, kinematic relocation systems known as 'Kelvin Clamp' have widely been used for well over a century, highly effective technique to provide an economical and dependable method with the precision engineering [5-6] such as the ultra-precision positioning and relocation of opto-mechanical components, metrological application, scientific apparatuses, the assembly of micro- and nano-parts as well as the high-precision tools [7]. By far, the most common form of standard kinematic couplings are three balls which are rigidly affixed to one part located to V-groove in the second component as shown in the typical structure below in Figure 1 [2].

In traditional kinematic coupling, every ball has two contact points with the V-groove, implying a small contact force and low stiffness. This involves six relatively rigid body degree of freedom in space between the two bodies by Hertzian contact, three translations ( $x, y, z$ ) and three rotations ( $\theta_x, \theta_y, \theta_z$ ) must be constrained [8]. Provided that more than six contact points exist, the system can be stiffer but will also be overconstrained, which will prevent modelling the structure in a closed form, more cost, increase the chance of manufacture errors, and of contamination from machine environments degrading reputability. The resulting connection will have some stiffness, accuracy and repeatability [9-10]. The local contact areas typical of these kinematic coupling are quite small and require a Hertzian analysis to ensure a robust design.

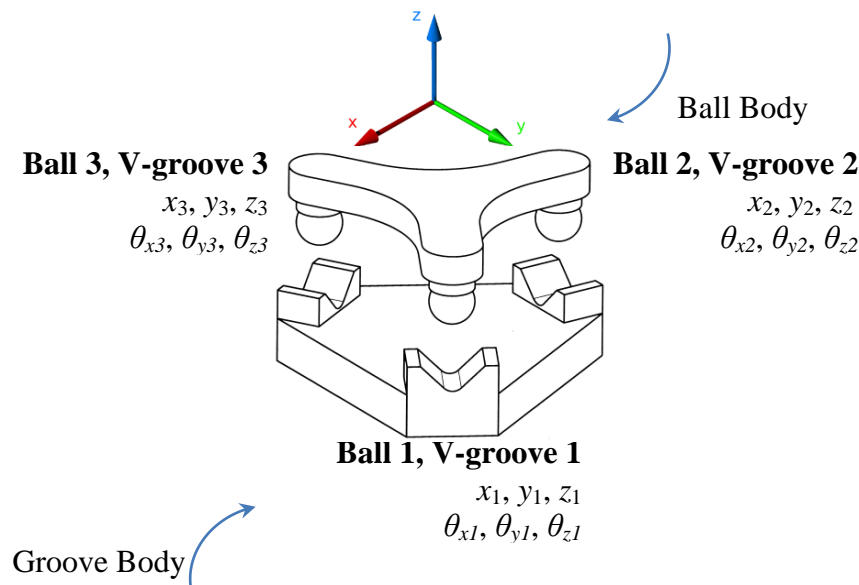


**Figure 1:** Kinematic coupling design with three V-grooves and three balls [2]

In the literature, published analyses and performance data relating to large devices, e.g., kinematic couplings, suggest that removal and replacement typically relocates to within 100 nm under well-controlled mounting conditions, e.g. [11-12]. Perhaps surprisingly, when seeking ways to precisely remove, measure and replace small samples within a micro- and nano-tribometer, it appears to be no authoritative public data on factors such as relocation repeatability for devices characterised by overall dimensions of a few millimetres or even smaller. Therefore, concentrating on kinematic arrangements using three balls and three V-grooves, this paper reports an experimental study of small-scale relocation precision stages and static stiffness of the clamps under various representative levels of closure force and cross-axis force, prompted originally by a need for relocation in the testing of very small tribological specimens.

## 2. Basic Assumptions of Hertz's Contact Stress Theory

The underlying principle behind kinematic relocation is Hertz contact [13]. Calculations are often based on the assumption of ideal Hertzian contact theory between two engineering surfaces as shown in Figure 2, where the top view of the contact area is circular. This generally accepted theory was presented by H. Hertz in 1881 [14-15] and summed up in many textbooks and handbooks [16-17-18-19]. It is convenient to sum up the Hertzian contact theory as calculations are often based on assumption of ideal Hertzian contact between the bodies. In this context, ideals mean [14-15-20-21]:

1. Both contacting surfaces are topographically smooth.

2. The contact of two bodies is frictionless, which implies that only a normal pressure is transmitted between them and the effect of surface shear stresses is neglected.
3. The dimensions of the radius of the contact circle must be small compared to the dimensions to each body (non-conforming elastic bodies) and to the radii of curvature of the contacting bodies.
4. Each body may be treated as an elastic half-space loaded over the plane elliptical contact area.
5. The stress disappears at great distance from the contact zone.

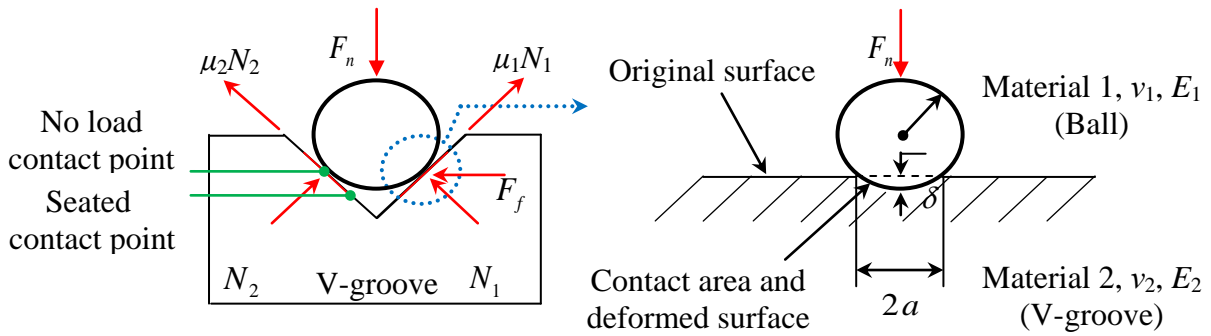


**Figure 2:** Schematic diagram of a ball in a V-groove

The applications of plane Hertz theory is based on the gap-bending hypothesis (for simple surface contact) states that the effect of geometry on the system in the contact region is a function of the algebraic sum of the curvatures of the two surfaces in contact [22-23]. Thus, the contact between two curved surfaces can be approximated by an equivalent contact problem between a sphere and a plane for which the solution is known [16]. In reality, normal contact of an elastic spherical ball on an elastic flat body will cause a deformation of both the flat body and the sphere [24-25]. Therefore, the first step, is to determine the equivalent Young's modulus of elasticity of the system based on the elastic moduli ( $E$ ) and Poisson ratios ( $\nu$ ) of the two bodies in contact assuming that the flat body is infinitely stiff, e.g. rigid, is given by

$$\frac{1}{E_e} = \frac{1 - \nu_{ball}^2}{E_{ball}} + \frac{1 - \nu_{flat}^2}{E_{flat}} \quad (1)$$

This illustrated in Figure 2, by a deformed ball on a flat surface. Next, the radius of an equivalent ball on a flat plate is given by

$$R_e = \frac{1}{R_1} + \frac{1}{R_2} \quad (2)$$

Where  $R_1$  and  $R_2$  are principle radii of curvature of two bodies. To minimize the effect on the contact zone stress, deflection should be as small as possible. As it is ball-on-flat configuration, a good compromise is to let, and,

$$R_e = R_{Ball} \quad (3)$$

The most well-known scenario is the contact region between an elastic ball and a flat surface as shown in Figure 2, where the top view of the contact area is circular and the total load,  $F_n$ , compressing a sphere of a radius,  $R$  into a flat surface can be related to the contact area,  $a$ , by

$$a = \left( \frac{3F_n R_e}{4E_e} \right)^{\frac{1}{3}} \quad (4)$$

The deflection (distance of approach of two far field points in the bodies) is given by

$$\delta = \frac{a^2}{R_e} = \left( \frac{9F_n^2}{16R_n E_e^2} \right)^{\frac{1}{3}} \quad (5)$$

When a tangential force  $F_T$  is applied to the sphere with respect to the flat-body, slip fronts will start to migrate inwards. A sliding contact will always have at least one contact point, which has stuck at all times from  $t = 0$ , if the tangential force  $F_T$  does not exceed the limiting friction force  $\mu F_N$  at any time  $t$ . The stiffness is also given by

$$\lambda_s = \frac{dF}{d\delta} = (6E_e^2 F_n R_e)^{\frac{1}{3}} \quad (6)$$

Equation no.6 is important as it shows that the interface stiffness depends upon the magnitude of the applied load. The Hertz contact stress (contact pressure) distribution is given by

$$P = P_o \left( 1 - \left( \frac{r}{a} \right)^2 \right)^{\frac{1}{2}} \quad (7)$$

Hence,  $P_o = \frac{3F_n}{2\pi a^2}$  is the maximum contact pressure at  $r = 0$

$$P_o = \left( \frac{6F_n E_e^2}{\pi^3 R_e^2} \right)^{\frac{1}{3}} \quad (8)$$

Referring back to Figure 2, approximately  $F_{n,ball} = F_{closure} / 3$ . Thus, at rest where no load is applied, there will be no friction force loading. Therefore,  $N_1 = N_2$ , then

$$N_1 = N_2 = \frac{F_n}{2 \cos \theta} \quad (9)$$

At applied load and move forward, then  $N_2$  will be at rest

$$N_1 = \frac{F_n}{\cos \theta} + F_f \quad (10)$$

$$N_1 = \frac{F_n}{\cos \theta} - F_f \quad (11)$$

The equations are well-known and incorporated into many different analysis tools, but it is important for designers to remember the overall relation for Hertz contacts.

### 3. Rational and design for the experimental scheme

For the planned applications, the relocation mounts must be physically small, low mass (for good dynamic systems) and low cost. Hence, samples have two orthogonal V-grooves to mate with a fixed set of balls. The elastic modulus and surface roughness will affect the relocation quality and stiffness against both normal and transverse load fluctuations. However, aluminium has attractively low density and not excessively expensive, while polishing the small groove features adds considerable cost. Thus, the coupling triangle, showing coupling centroid and centroid frame directions is shown in Figure 3 and the test-rig design and the sample parameters are set up as shown in Figure 4 and Table 1. Roughly speaking, the overall design of the test-rig combines cost-effective with simplicity of manufacturing. It also provides a clear and easy access for the specimen's replacement. At this stage of investigation, three archetype test-pieces have been used namely, mild steel or duralumin alloy blocks, with some duralumin samples then polished 'as well is economically reasonable' by a specialist company. Moreover, the design considered the use of stainless steel balls which are currently commercially available.

Slocum in [11] reports that when non-stainless steel components are used, one must be wary of fretting at the contact interfaces so steel coupling should only be used for low cycle applications. Although balls with fine surface finish are generally inexpensive, grooves with fine surface finish are expensive. The finishing operations used to prepare groove surfaces add considerable cost to kinematic.

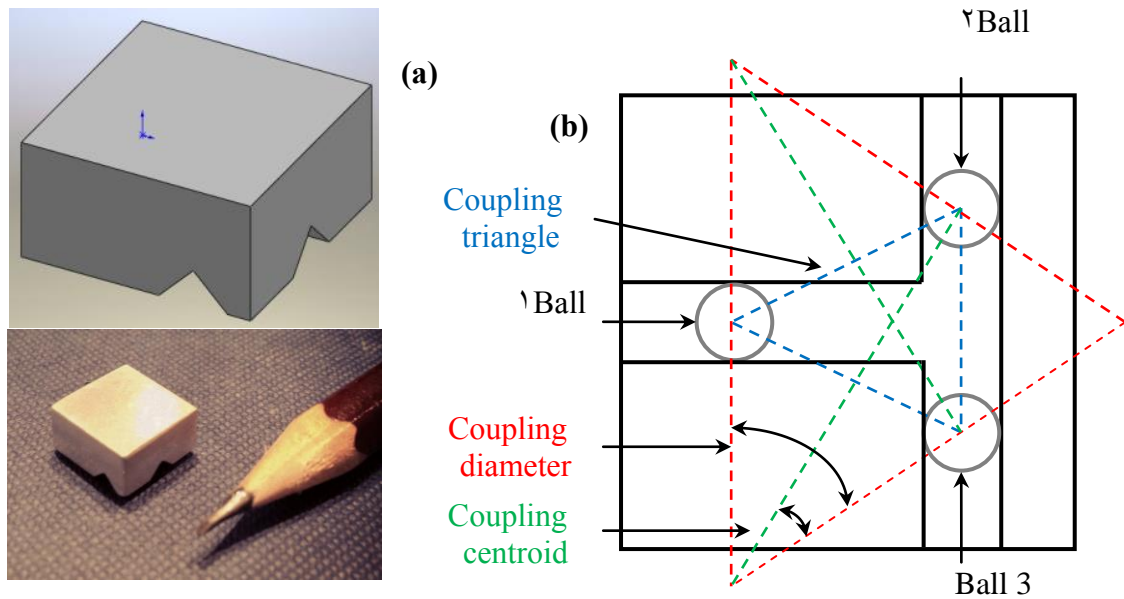


**Figure 3:** (a) 3D V-groove sample and (b) T-geometry groove pattern (coupling, triangle, coupling centroid and centroid frame directions). For good stability in the three-groove kinematic coupling, the normal to the planes containing the contact force vectors should be bisect to angles between the balls.

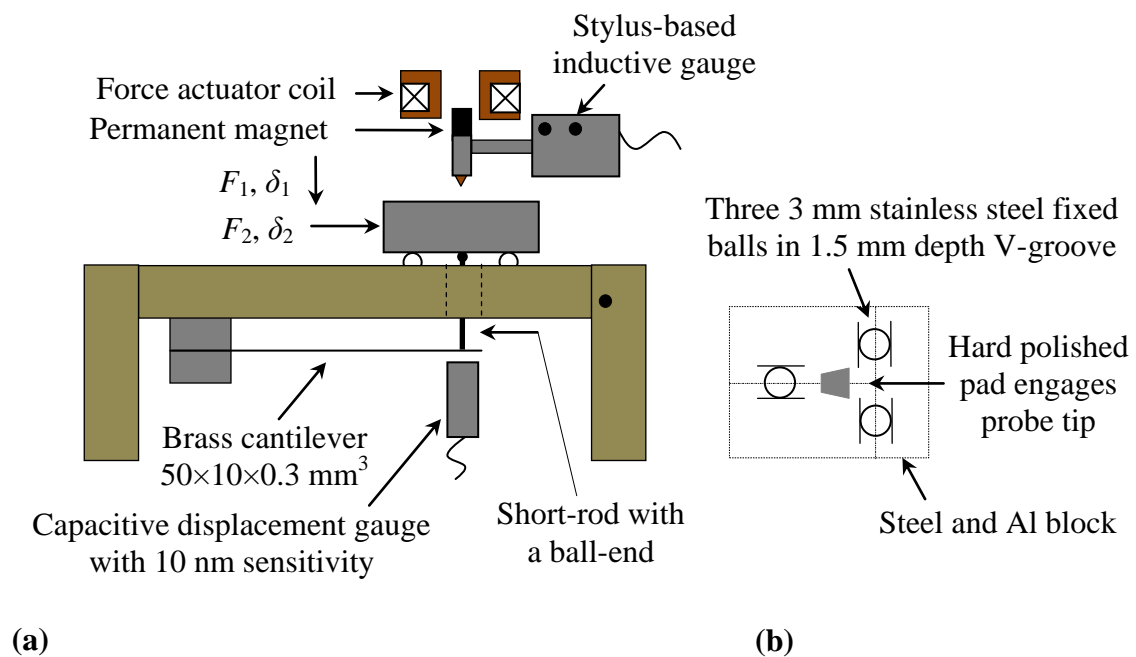


**Figure 4:** Test-rig: (a) overall schematic and (b) sample T-geometry groove pattern

**Table 1:** Summarization of parameters for Steel, Al and polished Al

Parameters	Steel	Al	Polished Al
Weight, $W_o$ (mN)	36	12.5	12.3
Roughness, $R_a$ (nm)	280	690	276
$R_q$ (nm)	360	949	366
$R_t$ ( $\mu\text{m}$ )	6.6	14.1	3.1
Modulus of Elasticity (GPa)	210	71	71
Added Camp Weights (g)		0, 2, 5, 10	
Applied Force (mN)		0.05, 0.1, 0.2, 0.5, 1.0, 1.5, 2.0	
Up-thrust (mN)		0.94	
Temperature ( $^{\circ}\text{C}$ )		$20 \pm 1$	
Relative Humidity (%RH)		$40 \pm 5$	

Figure 4 shows the test-rig concepts. Three 3 mm diameter stainless steel fixed balls with fine surface finish (standard commercial grade and inexpensive) are glued to a rigid steel outer frame. It is worth mentioning that stainless steel ball is an outstanding property which has a high modulus of elasticity, giving it very good stiffness (nearly three times that of as-ground aluminium). The test-piece of platform is placed onto the balls from the above with 1.5 mm deep  $90^{\circ}$  fine-ground grooves, so its vertical location is measured from below, challenging at the size and precision required. Typically, the separation between balls contacts is around 5 mm. In all cases, a bespoke test-bed enables convenient and adequately precisely located displacement metrology to well below 10 nm (that is, to considerably better than the repeatability expected for larger, more tractable Kelvin Clamps. Essentially, low-stiffness flexures are used to transfer movement at small contact probes to flat targets large enough to accommodate conventional capacitive displacement sensing.

Since not all the closure and modulating forces can be body forces, care must be taken to avoid uncertainties from strains induced by tractions. A capacitive displacement gauge (4810 capacitive gauges, ADE technologies) providing better than 10 nm sensitivity, monitors a weak brass cantilever beam ( $50 \times 10 \times 0.3 \text{ mm}^3$ ), to which is attached a short rod with a ball-end, projecting through a hole in the base. This capacitive gauge has been used with output voltage  $\pm 10 \text{ V}$ , output range  $\pm 50 \mu\text{m}$  and linearity  $\pm 10.77 \text{ nm}$  ( $\pm 0.0108\%$ ). This output is the standard analogue output and the voltage increases and decreases with the distance by moving the probe do that the gap between the target increases by the total measurement range. It is also vital that the probe and the target be parallel or error will occur. A hard polished pad on the platform (here, a small piece of a polished silicon wafer) touches this rod, always pushing down the leaf-spring and resulting in a small up-thrust on the platform. A stylus-based inductive gauge (Talysurf 5-120), having electromagnetic control of the contact force, engaged, vertically or horizontally the top or the edge of the platform, the force could again be set much lower than the weight.

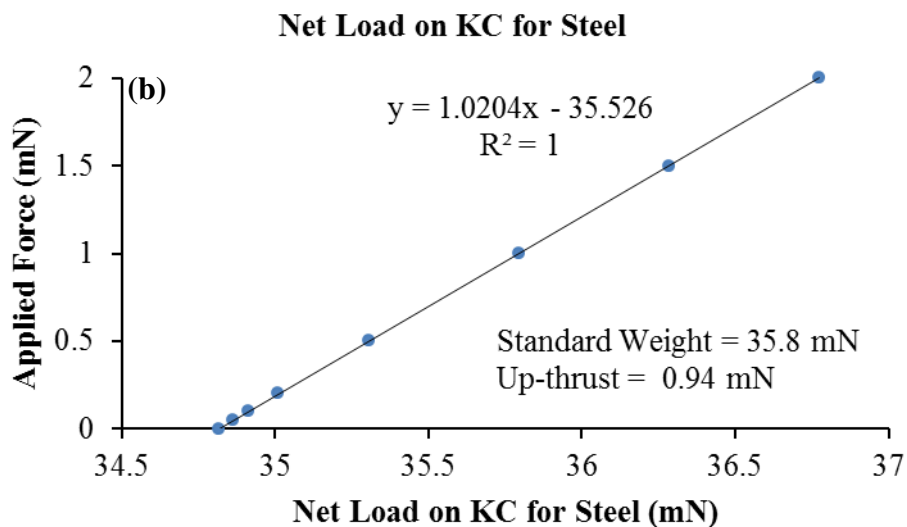
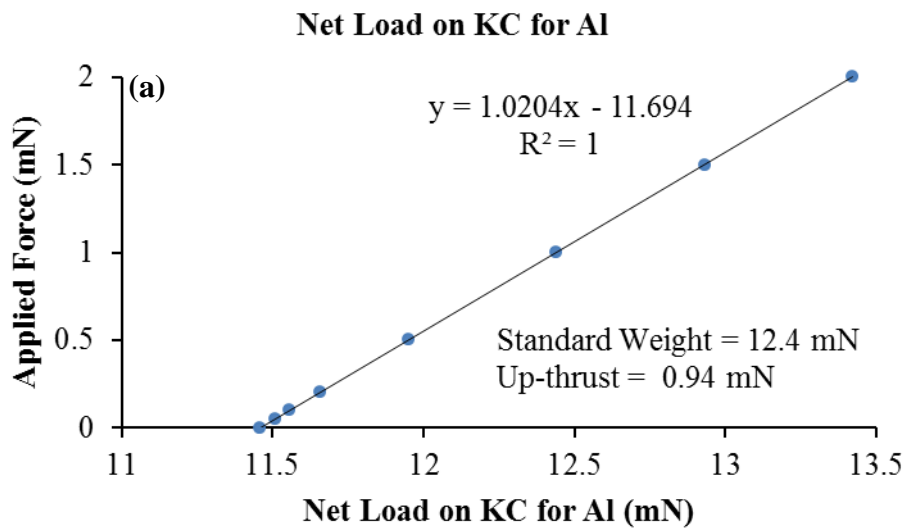
External current source (Knick, DC-Current-Calibrator J152) connected to force actuator coil in order to apply appropriate current, so that the desired field could be achieved. It mainly measured lateral displacement and through force modulation local stiffness (after checking for indentation error, especially on aluminium specimens). Extra dead-weight mass is added in order to the platform to adjust the nominal closure force of the clamp.

In this case, the up-thrust can be calculated using this formula

$$Up-thrust = (ball-ended\ push-rod) + (Glue) \quad (12)$$

Besides, the net load on the Kelvin Clamp can be calculated by using this formula, see Figure 5.

$$Net\ load\ of\ the\ KC = (Weight\ of\ device + Extra\ load) - (Up-thrust) \quad (13)$$



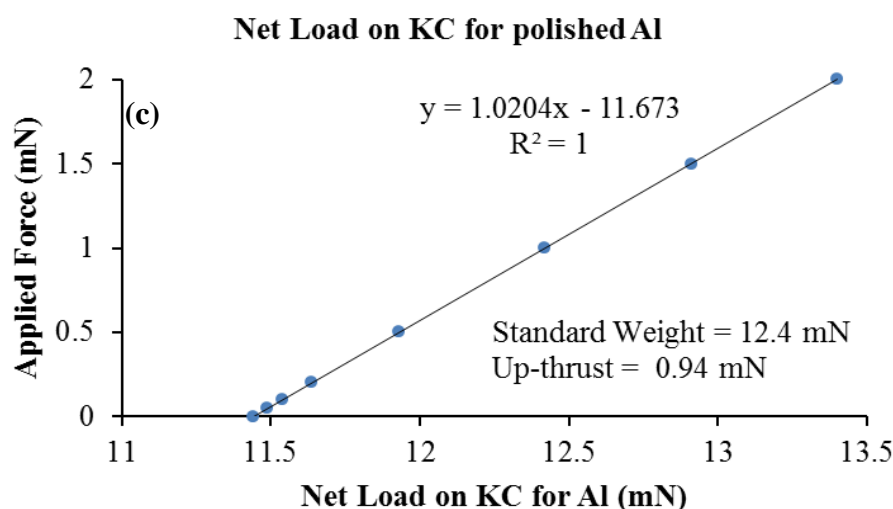


**Figure 5:** Net load of the KC (a) Al sample (b) Steel Sample and (c) polished Al sample

#### 4. Cleaning Procedure

It is of the utmost significance before starting the experiments to clean the specimens of any surface contaminants, such as dust, grease, or any other soluble organic particles so that there will be no adverse effect on the results. To achieve this, all specimens were ultrasonically cleaned with organic solvents (ethyl alcohol) for 15 minutes and this was followed by warm air drying. After cleaning, the specimens were stored for 24 hours in the same environment that will be used for the testing to allow the sample surface condition to equilibrate with the environment. The procedure described above was judged to be adequate at this stage. Figure 6 shows different surface topographies (some of them quite rough compared to common design practice) and materials for the grooves since these are critical factors for contact mechanics (and so of the clamp performance) as well as for the cost and applicability of small devices.

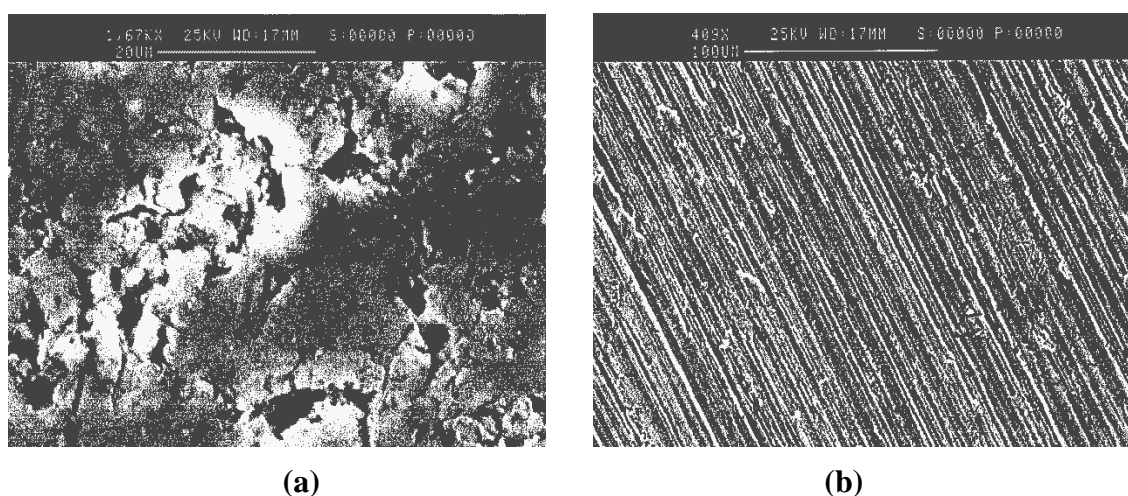


**Figure 6:** Surface topography of (a) Al sample (b) Steel Sample using Scanning Electronic Microscopy SEM

## 5. Calibration Procedure

The calibration procedure is classified in calibrating the cantilever beam stiffness and the external current source for applying the various loads. The capacitive gauge was directly calibrated by applying different normal weights on the vertical position, as shown in Figure 7. For convenience, three calibration trials have been carried out. Dead-weight calibration showed that the cantilever beam was linear spring ( $R^2 > 0.999$ ), so the up-thrust was readily derived from the gauge reading. The up-thrust was held always below 1 mN. Displacement gauges were calibrated against step artefacts, leading to absolute uncertainties of 5 - 8 % of reading. This is adequate as these trials are predominantly about relative behaviour; design interpretation to other systems is always vulnerable to variations in materials and dimensions.

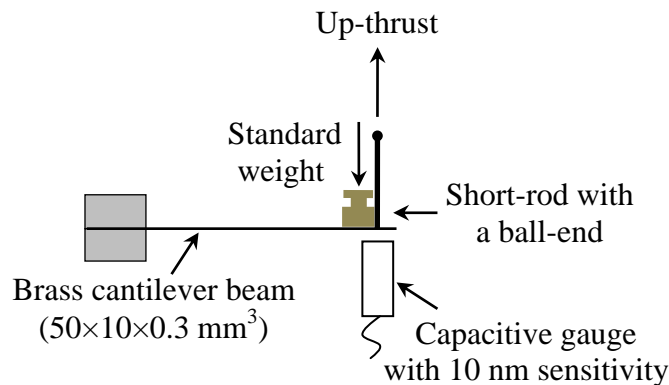


**Figure 7:** Schematic diagram of measuring the cantilever beam stiffness

## 6. Repeatability Relocation Performance

As mentioned above, in high-precision applications, the repeatability of the kinematic couplings has to be addressed, particularly those to be removed for micro-tribometer and precisely relocated to their original position [26]. So, at the beginning of the test, the platform was mounted onto the fixed three 3 mm stainless steel balls in 1.5 mm depth V-groove and the relevant displacement gauge set against it. In this case, the platforms (steel and as-ground aluminium) were repeatedly gently removed and replaced in the same orientation 10 times (using tweezers in order to minimise the thermal effects), with the capacitive gauge reading recorded each time. After that, tests were repeated 10 times with additional masses of 2, 5, and 10 g lightly glued to the platform on order to obtain lower scatter. The following sub-sections will discuss the performance of relocation on both horizontal and vertical positions for Al, steel and polished Al.

### 6.1 Vertical Relocation of the T-geometry Clamp

This type of repeatability was carefully investigated through the test with different combinations of load, material and surface roughness. Figures 8 and 9

show the results from the set of 40 tests for the steel and as-ground aluminium platforms, with error bars showing the standard deviations. Consistent with Hertzian contacts, the mean position shifts by diminishing amounts as the total weight increases. Steel samples showed around 70% lower displacements for the same weight change. The total load had little effect on the relocation about the mean height. It has been assumed that the behaviour at interface asperities was frictionless, but as long as steel was used, friction would be present and the danger of fretting would be exists. This is, to some extent, true at high load. However, for small size contact and light load, friction can be neglected in which the dimension of the contact area is small compared with the radii of curvature and the dimensions of the involved bodies. On this basis, the steel device relocated to within  $\pm 70$  nm with 95% confidence, the aluminium one to within  $\pm 130$  nm, reflecting its lower Young's modulus and rougher grooves against both normal and transverse load, as expected.

The polished aluminium sample gave results only a little better than the as-ground one, which means that high surface finish needs to be around 0.1 nm. However, Polishing aluminium adds considerable cost, time and needs very sophisticated machine to polish the surface at small scale. Generally speaking, with respect to scatter in the data (for both steel and as-ground aluminium), results show steel device nearly three time that as-ground aluminium device at various loads. Moreover, the footprint of stainless steel balls on as-ground aluminium device would be about half that of stainless steel balls on steel device at various applied loads.

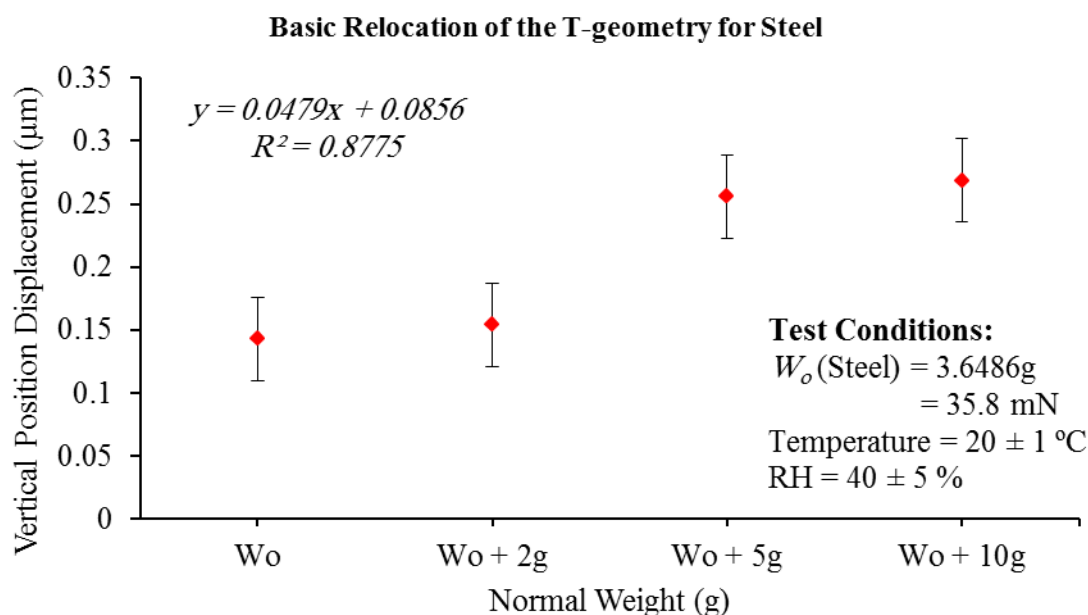


**Figure 8:** Vertical repeatability of steel device at various loads

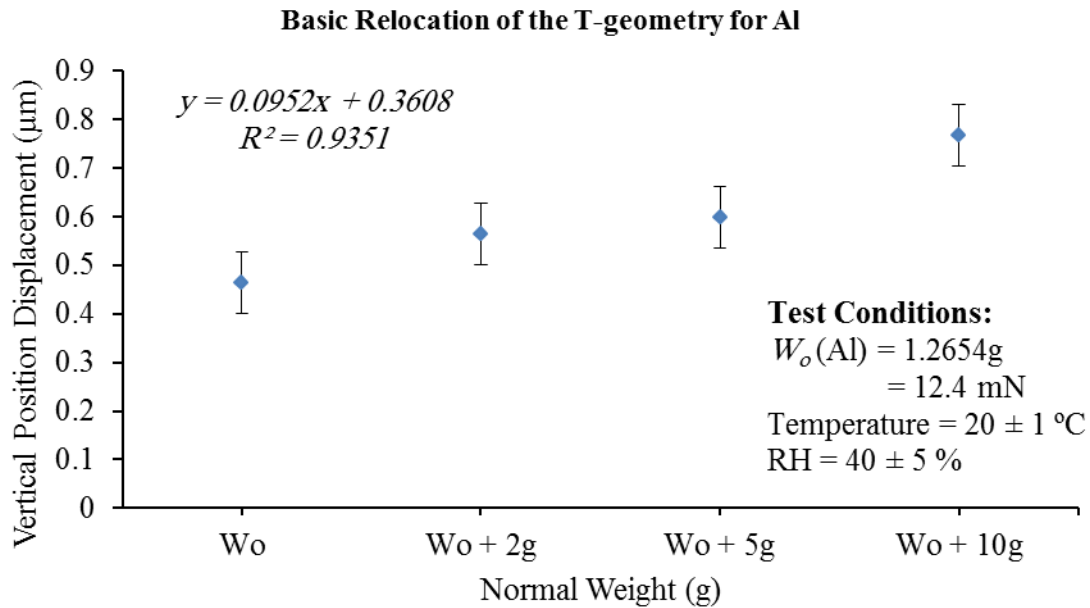


**Figure 9:** Vertical repeatability of aluminium device at various loads

## 6.2 Horizontal Relocation of the T-geometry Clamp

In a way similar to vertical relocation, horizontal relocation is measured with the same step. By using stylus based inductive gauge, horizontal relocation was tested on the presumed most vulnerable axis, parallel to the groove located on the two fixed balls (the direction of the weakest constraint). As the lateral position was restricted with applying the load, tests were repeated with additional masses of 5, 10, 20, 50, 100, 150 and 500 mg. Figures 10 and 11 show the results from the set of 10 tests for the steel and as-ground aluminium platforms, with error bars showing the standard deviations. All samples are located unreliably at lateral forces above a few tens of mN, predominantly because of a tilting from  $\sim 2\text{ mm}$  Abbe offset of the force above the contact plane (typical applications might suffer from larger offsets). With sub-mN stylus force, 95% confidence relocation was  $\pm 140\text{ nm}$  and  $\pm 230\text{ nm}$  for steel and as-ground aluminium samples, essentially independent of extra load up to 10g or lateral forces up to 20 mN. Wear marks have been shown on the device (for both, steel and as-ground aluminium) due to the sliding of stainless steel balls into and along the grooves during centring the devices. The wear changes the surface geometry by the order to tens of microns or sub-microns. Surprisingly, the most notable work to reduce ball-groove wear was done by Slocum and his colleagues who used lubricated silicon nitride balls [6].

Again, as the cost is an issue, it prevents them for being used in high-precision engineering. It is worth mentioning here, as the load increased, further deforming surface asperities will take place.

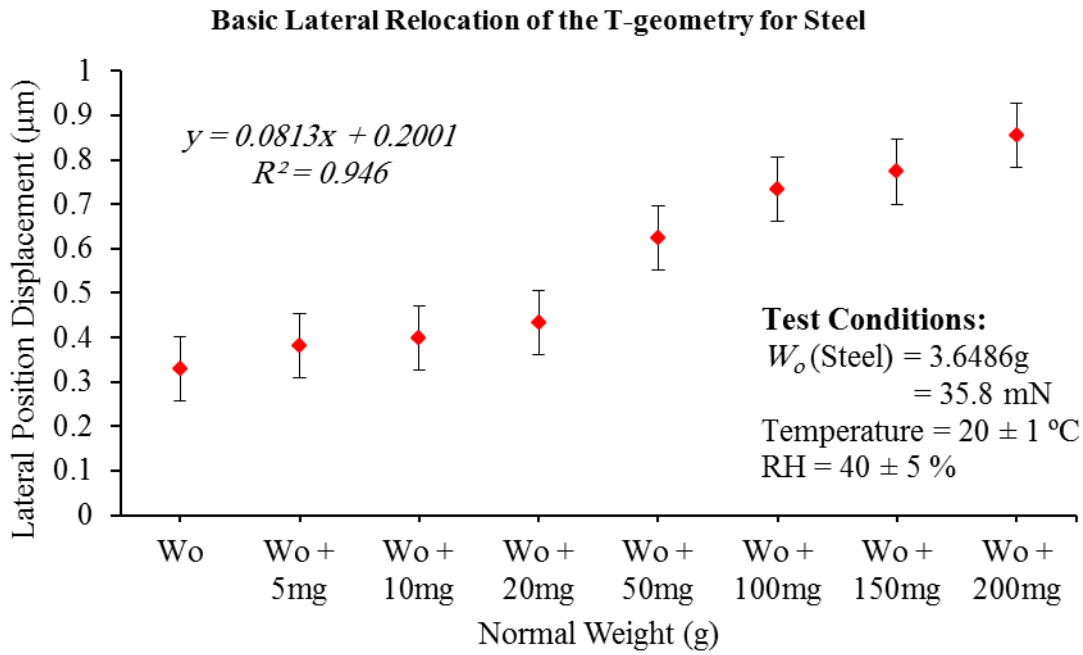


**Figure 10:** Lateral repeatability of steel device at various loads

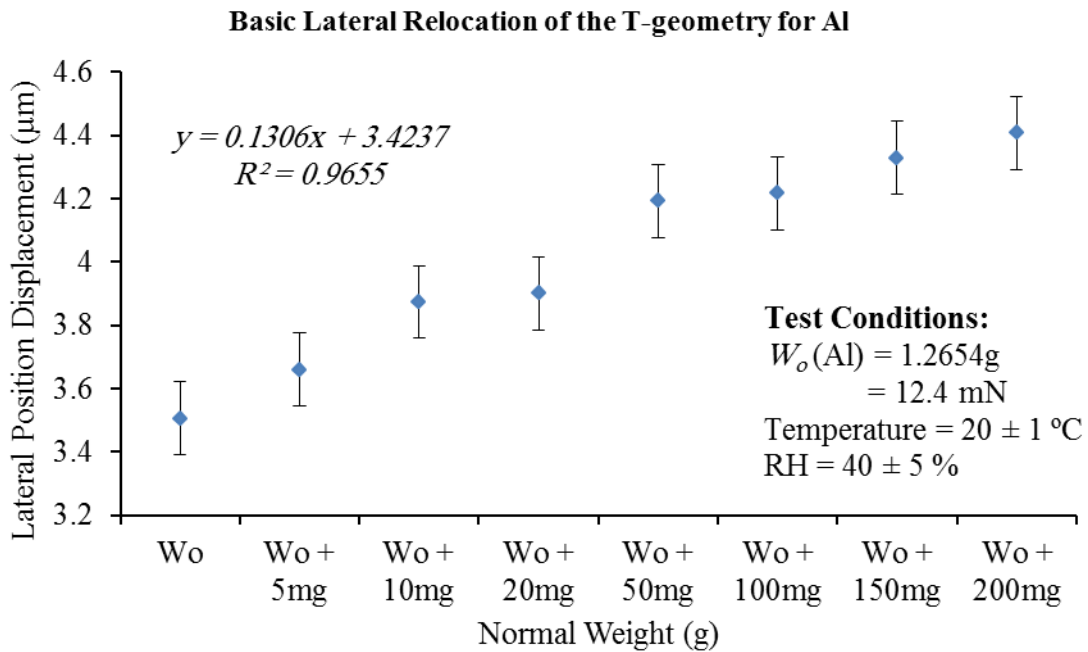


**Figure 11:** Lateral repeatability of aluminium device at various loads

### 7. Local Stiffness of T-geometry Clamp

Locating the platform, setting the vertical gauge and then gently adding and removing dead-weights of 2 g, 5 g or 10 g, without removing the platform itself resulted in curves for mean height against load broadly similar to those in figures 8 and 9. For steel, the standard deviation was consistently around 30 nm (notably

lower than that for relocation, as expected). However, the standard deviation with aluminium was similar to that for relocation. This is attributed to greater swapping of the actual ball contacts between asperities on the softer, rougher material. Over a 98 mN imposed range, vertical stiffness were approximately 1100 mN/μm for steel device and 190 mN/μm for as-ground Al. Figure 12 illustrates the basic vertical deflection of the steel and as-ground aluminium. The plots show a generally consistent increase in the resultant elastic deformation with contact load on each surface. Moreover, it shows that the surface with low roughness has smaller deflection than those of high roughness surface at repeated load. Even for the same Hertzian contact, the plastic deformation state behaves differently depending on the roughness of the surface. Basic vertical and lateral stiffness between any two points (e.g., A and B points) can be given by

$$k = \frac{\Delta F}{\delta_z}(W_o) \quad (14)$$

And also, between (e.g., B and C points) can be given by

$$k = \frac{\Delta F}{\delta_z}(W_o + \text{extra weight}) \quad (15)$$

Figure 13 illustrates horizontal deflection in the most vulnerable axis against forces up to 2 mN, using self-weight as the vertical closure force. The horizontal stiffness for both steel and as-ground aluminium was around 20 mN/μm. Significant improvement is possible with an extra 10 g closure load, this changed to around 25 mN/μm and 10 mN/μm as shown in Figure 14. The anomalous behaviour result for aluminium seems due to residual tilting effects at the small closure force, and no significant difference between their deflections that correlates to the roughness difference between them. Polished aluminium behaved quite similarly to the steel throughout. In general, the effect of roughness on such deflection was not very obvious.

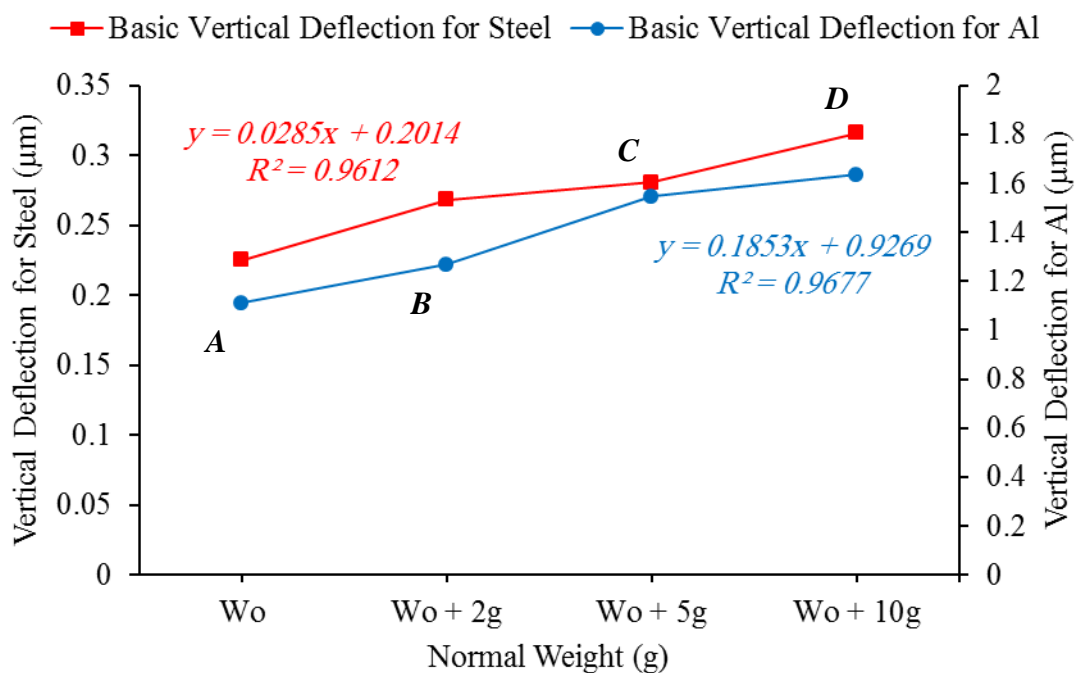


**Figure 12:** Vertical deflection with force under self-weight closure for the steel and as-ground aluminium

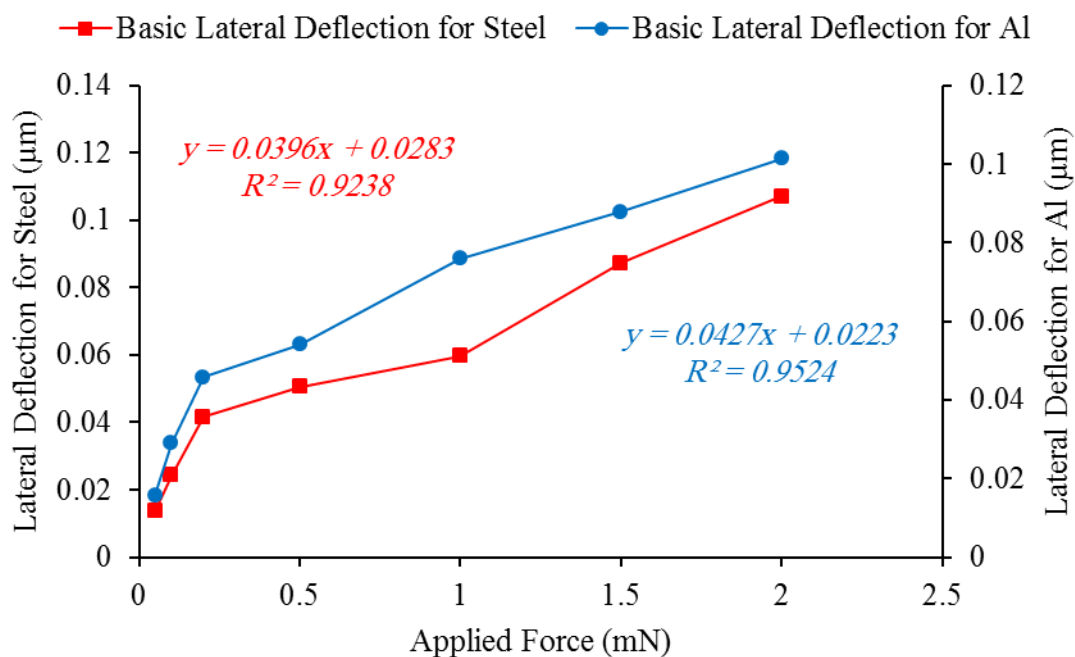


**Figure 13:** Lateral deflection with force under self-weight closure for the steel and as-ground aluminium

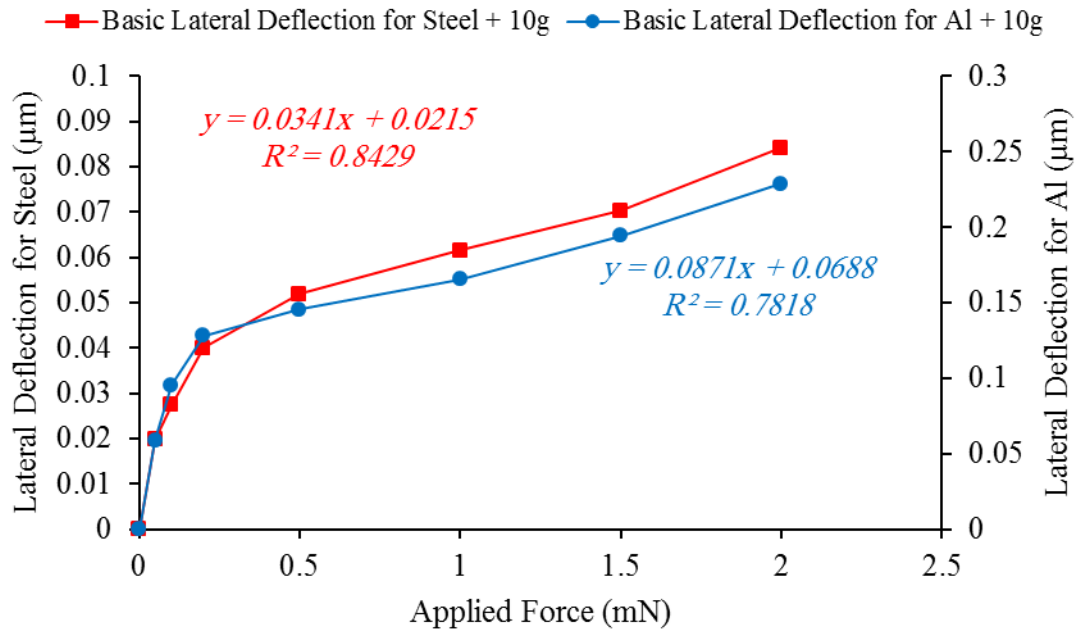


**Figure 14:** Lateral deflection with force under self-weight closure for the steel and as-ground aluminium + 10g

## 8. Concluding Remarks

Kinematic couplings are known as economical method for precisely locating one body with respect to another body. The preliminary investigations accomplished and based on the available experimental results of the research, the following conclusions were made concerning the performance of a three 3 mm stainless steel balls with fine surface finish in a 1.5 mm depth V-groove of steel and as-ground aluminium platforms:

- **Vertical Relocation of T-geometry:** the steel device relocated to within  $\pm 70$  nm with 95% confidence, the Al one to within  $\pm 130$  nm. The polishing Al sample gave results only a little better than the as-ground one.
- **Horizontal Relocation of T-geometry:** with 95% confidence, the relocation was  $\pm 140$  nm and  $\pm 230$  nm for steel and as-ground Al samples, essentially independent of extra normal load up to 10 g or lateral forces up to 20 mN.
- **Local Stiffness of T-geometry:** vertical stiffness was about 1100 mN/ $\mu$ m for steel and 190 mN/ $\mu$ m for as-ground Al. The horizontal stiffness was around 20 mN/ $\mu$ m for both platforms. With 10 g extra closure load, this changed to around 25 mN/ $\mu$ m for steel and 10 mN/ $\mu$ m for as-ground Al. The anomalous results for Al seem due to residual tilting effects at small closure force. Polished Al behaved quite similarly to steel platform.

Thus, it seems that these small Kelvin clamps were relocated to  $\pm 250$  nm or even better both vertically and horizontally in the ambient conditions. This is indeed a little worse than reported for the larger systems, but encouragingly good for a great many applications. Horizontal stiffness with T-geometry grooves is much lower than

the vertical value. However, even the low-mass; low-cost aluminium device was stiff enough for, e.g., many micro-tribometer applications, although horizontal behaviour was very sensitive to the closure force. Therefore, low-cost millimetre-scale Kevin clamp are practicable, with care. The finishing operations used to prepare groove surfaces add considerable cost to kinematic couplings. So, polished grooves appear not to be cost-effective improvements for low-mass devices. It must be realized that kinematic relocation method can result in coupling with extremely high accuracy, but with limited applied load at potentially lower cost.

Future work should consider expanding the techniques discussed in this paper to set up similar investigation using 120°-geometry for both steel and as-ground aluminium as the test-rig designed was capable of giving very useful information concerning these small devices kinematic relocation systems.

**Reference:**

- [1] Maxwell, J. C. (1890). General considerations concerning scientific apparatus in the scientific papers of James Clerk Maxwell. ed. W. D. Nivens, Dover Press.
- [2] Slocum, A. H. and Halea, L. C. (2001). Optimal design techniques for kinematic couplings. *Precision Engineering*, 25, 114-127.
- [3] Evans, Chris J. (1989). Precision Engineering: an evolutionary view. Granfield, England, Granfield Press.
- [4] Thompson, W, Tait, P. G. Treatise on Natural Philosophy, Cambridge, (1879). Reprinted as Principles of Mechanics and Dynamics, Dover Publications, New York, 1912:1962.
- [5] Slocum, A. H. (1988). Kinematic couplings for precision fixturing – Part 1: formulation of design parameters. *Precision Engineering*, 10, 85-91.
- [6] Slocum, A. H. and Donmez, A. (1988). Kinematic couplings for precision fixturing – Part 2: Experimental determination of repeatability and stiffness. *Precision Engineering*, 10, 115-112.
- [7] Zelenika, S. and Flechsig, S. (2002). Kinematic coupling for synchrotron radiation instrumentation. *Proc. 2<sup>nd</sup> International Workshop on Mechanical Engineering Design of Synchrotron Radiation Equipment and Instrumentation (MEDSI02)*. 262-270.
- [8] Schouten, C. H., Rosielle, P. C. J. N. and Schellekens, P. H. J. (1997). Design of a kinematic coupling for precision applications. *Precision Engineering*, 20, 46-52.
- [9] Culpepper, M. L. (2004). Design of quasi-kinematic couplings. *Precision Engineering*, 28, 338-357.
- [10] Hart, A. J., Slocum, A. and Willoughby, P. (2004). Kinematic coupling interchangeability. *Precision Engineering*, 28, 1-15.
- [11] Slocum, A. H. (1992). Design of three-groove kinematic couplings. *Precision Engineering*, 14, 67-76.
- [12] Willoughby, P. J., Hart, A. J. and Slocum, A. H. (2005). Experimental determination of kinematic coupling repeatability in industrial and laboratory conditions. *Journal of Manufacturing Systems*, 24, 108-121.
- [13] Johnson, K. L. (1982). One hundred years of hertz contact. *Proc. Instn. Mech. Engrs.*, 196, 363-378.
- [14] Deeg, E. W. (1992). New algorithms for calculating Hertzian stresses, deformations and contact zone parameters. *AMP Journal of technology*, 2, 14-24.
- [15] Antoine, J-F., Visa, C., Sauvey, C. and Abba, G. (2006). Approximate analytical model for Hertzian elliptical contact problems. *Journal of Tribology*, 128, 660-664.

- [16] Slocum, A. H. (1992). Precision machine design. 1<sup>st</sup> edition. USA, Prentice-Hall, Inc.
- [17] Young, W. C. and Budynas, R. G. (2002). Roark's formulas for stress and strain. 7<sup>th</sup> edition. Singapore, McGraw-Hill.
- [18] Timoshenko, S. P. and Goodier, J. N. (1970). Theory of elasticity. 3<sup>rd</sup> edition. New York, McGraw-Hill.
- [19] Smith, S. T. and Chetwynd, D. G. (1992). Foundations of Ultraprecision mechanism design. 1<sup>st</sup> edition. USA, CRC Press.
- [20] Houpert, L. (2001). An Engineering Approach to Hertzian Contact Elasticity – Part I. *Journal of Tribology*, 123, 582-588.
- [21] Houpert, L. (2001). An Engineering Approach to Non-Hertzian Contact Elasticity – Part II. *Journal of Tribology*, 123, 589-594.
- [22] Greenwood, J. A. (1997). Analysis of elliptical Hertzian contacts. *Tribology International*, 30, 235-237.
- [23] Sackfield, A. and Hills, D. A. (1983). Some useful results in the classical hertz contact problem. *Journal of Strain analysis*, 18, 101-105.
- [24] Van Veggel, A. A. and Nijmeijer, H. (2009). Stable mounting of beamsplitters for an interferometer. *Precision Engineering*, 33, 7-17.
- [25] Jamari, J. and Schipper, D. J. (2007). Deformation due to contact between a rough surface and a smooth ball. *Wear*, 262, 138-145.
- [26] Slocum, A. (2010). Kinematic couplings: a review of design principles and applications. *International Journal of Machine Tools and Manufacture*, 50, 310-327.